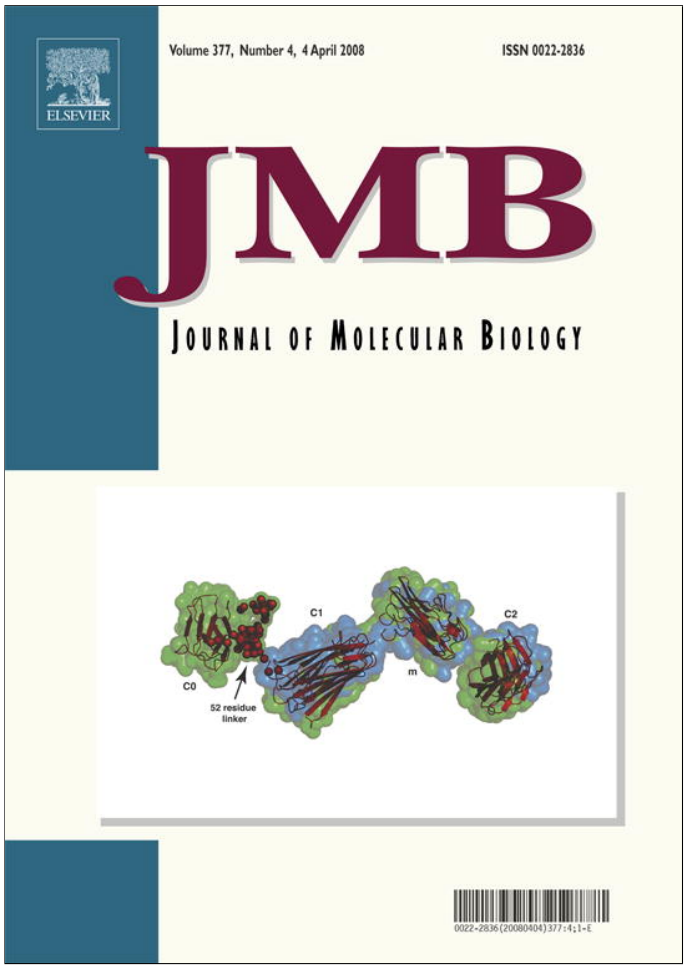

doi:10.1016/j.jmb.2008.01.055 J. Mol. Biol. (2008) 377, 1251–1264

JMB

Available online at www.sciencedirect.com

ScienceDirect

ELSEVIER

A Logical OR Redundancy within the As*x*-Pro-As*x*-Gly Type I β-Turn Motif

Jihun Lee, Vikash Kumar Dubey, Liam M. Longo and Michael Blaber*

Department of Biomedical Sciences, College of Medicine, Florida State University, Tallahassee, FL 32306-4300, USA

Received 6 December 2007; received in revised form 22 January 2008; accepted 22 January 2008
Available online 31 January 2008

Edited by P. Wright

Turn secondary structure is essential to the formation of globular protein architecture. Turn structures are, however, much more complex than either α-helix or β-sheet, and the thermodynamics and folding kinetics are poorly understood. Type I β-turns are the most common type of reverse turn, and they exhibit a statistical consensus sequence of As*x*-Pro-As*x*-Gly (where As*x* is Asp or Asn). A comprehensive series of individual and combined As*x* mutations has been constructed within three separate type I 3:5 G1 bulge β-turns in human fibroblast growth factor-1, and their effects on structure, stability, and folding have been determined. The results show a fundamental logical OR relationship between the As*x* residues in the motif, involving H-bond interactions with main-chain amides within the turn. These interactions can be modulated by additional interactions with residues adjacent to the turn at positions $i+4$ and $i+6$. The results show that the As*x* residues in the turn motif make a substantial contribution to the overall stability of the protein, and the As*x* logical OR relationship defines a redundant system that can compensate for deleterious point mutations. The results also show that the stability of the turn is unlikely to be the prime determinant of formation of turn structure in the folding transition state.

Keywords: β-hairpin; protein engineering; protein stability; protein folding; protein evolution

Introduction

Of the three fundamental types of protein secondary structure, only the reverse turn is nonlinear and permits formation of globular protein architecture. Reverse turns are also unique in that they are not described by a repetitive characteristic value of backbone ϕ,ψ angles, but rather, each category of reverse turn is defined by a unique sequential set of such angles. Richardson has characterized the β-turn as having six distinct types (I, I′, II, II′, VIa, and VIb), as well as a miscellaneous category (IV), based on main-chain ϕ,ψ angles.[1] If a β-turn connects two β-strands that form an antiparallel β-sheet, then it is known as a β-hairpin turn. Sibanda *et al.* developed an *X*:*Y* shorthand for β-hairpin structures, whereby *X* identifies the number of residues required for the turn and *Y* identifies the hydrogen-bonding pattern in the closure of the turn (*X* equals *Y* when the closure involves two backbone hydrogen bonds, whereas $Y=X+2$ if closure involves one hydrogen bond).[2] Sibanda *et al.* noted that the number of residues in β-hairpin turns typically comprises two to seven residues ($X=2$–7) and can be further classified according to different patterns of backbone hydrogen bonding. This complexity distinguished β-turns from the other types of secondary structure.

The type I 3:*Y* ($Y=3$ or 5) β-turn is one of the most prevalent types of β-turns in protein structures, representing approximately one-third of all β-turns.[2,3] The type I turn is defined by a characteristic set of sequential main-chain ϕ,ψ angles that result in an approximately 180° change in the direction of the peptide chain. Of the various subtypes in this category, the most common is the type I 3:5 G1 bulge β-turn. The initial residue in the turn is defined as residue *i*, and subsequent residues in the turn are indexed accordingly ($i+1$, $i+2$, etc.). In this turn, the residue at position *i* has main-chain angles typical of β-sheet secondary structure; residue $i+1$ is located

*Corresponding author. E-mail address: michael.blaber@med.fsu.edu.

Abbreviations used: WT, wild type; FGF-1, fibroblast growth factor-1; PDB, Protein Data Bank; GuHCl, guanidine HCl; ADA, *N*-(2-acetamido)iminodiacetic acid.

within the right-handed α-helical region; residue $i+2$ is located within the right-handed γ-helical region; residue $i+3$ is located within the left-handed γ-helical region; and residue $i+4$ has main-chain angles typical of β-sheet secondary structure. The shorthand for the characteristic type I 3:5 G1 bulge β-turn conformation is therefore sometimes given as "$\beta\alpha_R\gamma_R\gamma_L\beta$."[1,2]

A study of the positional frequency of amino acids in different turn types has identified statistical preferences for side-chain residues within type I turns.[4,5] These preferences include Asx (Asp or Asn) at position i, Pro at position $i+1$, Asx at position $i+2$, and Gly at position $i+3$. The Asx residues may be structurally important in the type I β-turn because they can participate in hydrogen-bonding interactions with specific backbone amides. An Asx residue at position i in a type I turn can satisfy the hydrogen-bonding requirement of the main-chain amide at positions $i+2$ and $i+4$ if it adopts a rotamer of $\chi_1 = +60°$ (*gauche*$^-$). Similarly, an Asx residue at position $i+2$ in a type I turn can satisfy the hydrogen-bonding requirement of the main-chain amide at position $i+4$ if the Asx adopts a *gauche*$^-$ rotamer (however, it cannot also satisfy the hydrogen-bonding requirement of the main-chain amide at position $i+2$). Furthermore, if Asx residues are present at both positions i and $i+2$, they cannot simultaneously adopt *gauche*$^-$ rotamers due to a steric clash.

The importance of the statistically preferred Asx residues at positions i and $i+2$ in type I 3:5 G1 bulge β-turns has been studied by several groups with regard to the contribution to protein or peptide stability and folding. As part of an effort to develop a useful β-turn "toolkit", Blandl *et al.* substituted the Pro-Asp-Gly tripeptide sequence into a 2:2 turn region of a disulfide-cyclized peptide that spontaneously folds into a β-hairpin.[6] NMR data indicated that the mutant turn adopted a type I 3:5 G1 bulge β-turn structure. Wan and Milner-White performed a statistical study of the most common types of hydrogen-bonding interactions between side-chain carboxylate/amide groups and main-chain groups.[7] The majority of such interactions can be characterized as involving Asx side chains in a hydrogen-bonding arrangement with the main-chain amide group's carboxy-terminus to the Asx. They identified six general categories of such "Asx motifs"; among these was the type I 3:5 G1 bulge β-turn. In this case, the Asx residue is present at position i and hydrogen bonds to the main-chain amide of turn positions $i+2$ and $i+4$. Another of the six identified categories of Asx motifs was the "Asx β-turn." In this arrangement, an Asx residue at position i hydrogen bonds to the main-chain amide of residue $i+2$. This structure is indistinguishable from an Asx at position $i+2$ in a type I 3:5 G1 bulge β-turn hydrogen bonding to the main-chain amide of turn position $i+4$. Thus, type I 3:5 G1 bulge β-turns can potentially incorporate one of two characterized Asx motifs. De Alba *et al.* and Santiveri *et al.* have studied two designed peptides that incorporate a centrally located Asn-Ser-Asp-Gly sequence.[8–10] NMR data indicate that these peptides form a β-hairpin structure, although the β-turn appears to interconvert between a type I 4:4 and a type I 3:5 G1 bulge β-turn. Molecular dynamics simulations of the same peptide sequences indicate a rapid collapse to a β-hairpin-like conformation, and that β-hairpin formation is initially driven by the bending propensity of the turn sequence.[10] These studies suggest that an Asx-Xxx-Asx-Gly sequence favors a β-turn conformation and is a key structural nucleation event that drives the folding of β-hairpin-containing proteins. In related work, de Alba *et al.* identified important electrostatic effects for the $i+2$ Asp in stabilizing the β-bulge turn structure, although the magnitude of the energetics was not determined.[11] Zerella *et al.* have studied a peptide representing the amino-terminal β-hairpin structure of ubiquitin, and formation of the native type I 3:5 G1 bulge β-turn structure within this region is thought to be an important early folding event.[12] In this regard, the wild-type (WT) turn sequence is Thr-Leu-Thr-Gly, and these investigators observed that mutation to Thr-Leu-Asp-Gly stabilized the β-turn structure substantially (from ~18% formation to ~64% formation). Jager *et al.* replaced the unusually long loop 1 within the Pin WW domain by a shorter sequence with a statistically preferred type I G1 bulge conformation (Asp at position $i+2$). They observed designed mutants exhibiting increased thermodynamic stability, with increased folding kinetics.[13] The above studies highlight important roles for the folding and stability of Asx residues at positions i and $i+2$ in type I 3:5 G1 bulge β-turns. These results show that Asx residues at positions i and $i+2$ are key elements for this type of turn to fold autonomously, function as a folding nucleus, or increase the overall rate of folding. Despite their critical contribution to protein folding and stability, details of the folding kinetics and thermodynamic contribution of Asp *versus* Asn, at both positions i and $i+2$ within such turns, are not known.

Fibroblast growth factor-1 (FGF-1) is a member of the β-trefoil superfold (exhibiting a characteristic 3-fold tertiary structure symmetry). It is composed of β-strand and turn secondary structure that can be described as forming a six-stranded β-barrel closed off at one end by three β-hairpins.[14,15] The β-hairpin structures that close off the end of the β-barrel (i.e., turns 2, 6, and 10; Fig. 1) each contain a solvent-exposed type I 3:5 G1 bulge β-turn. The Gly residue at position $i+3$ within these turns (residue positions 29, 71, and 115) is highly conserved in the FGF family of proteins (87–100% conserved among 23 members). This degree of conservation likely reflects the important role of the Gly residue in stabilizing the type I 3:5 G1 bulge β-turn. However, apart from the $i+3$ Gly, the primary structures within turns 2, 6, and 10 of FGF-1 are different and consist of Leu-Pro-Asp-Gly (LPDG), Asp-Thr-Asp-Gly (DTDG), and Lys-Lys-Asn-Gly (KKNG), respectively. Thus, while no individual turn contains the type I β-turn

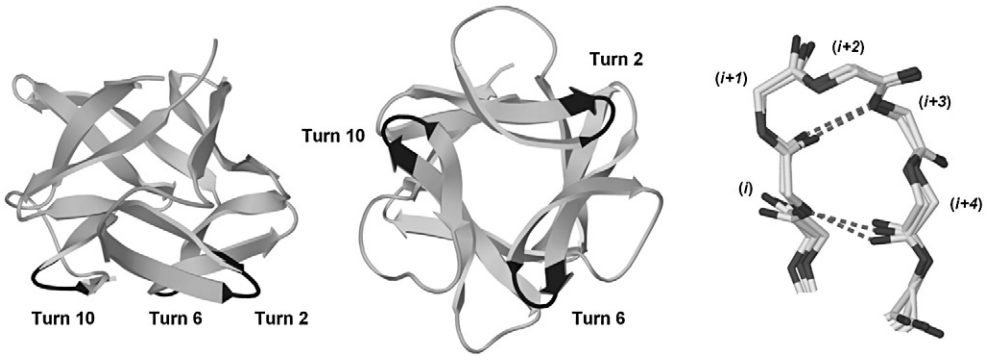

Fig. 1. Ribbon diagram of FGF-1 from side view (left panel) and bottom view (middle panel) showing the location of type I 3:5 G1 bulge β-turns 2, 6, and 10 (dark regions). A main-chain overlay of these turns (showing H-bonds and turn positions) is shown in the right panel.

consensus sequence of As*x*-Pro-As*x*-Gly, each turn contains various elements of the consensus sequence, and all contain a consensus As*x*-Gly at positions $i+2$ and $i+3$, respectively.

These three type I 3:5 G1 bulge β-turns in FGF-1 have been subjected to a comprehensive series of Asp and Asn mutations at positions i and $i+2$ (including Ala reference mutations), and the effects on structure, stability, and folding have been determined. For each turn, the following mutants were studied: four single mutants (NA, AN, DA, and AD), four double mutants (NN, ND, DN, and DD), and the double Ala reference mutant (AA), where the first letter (using the single-letter amino acid code) denotes the residue at position i and the second letter denotes the residue at position $i+2$. In all the mutants, the corresponding WT $i+1$ and $i+3$ residues were maintained. The results, while complex, indicate that the fundamental interaction between the As*x* residues at positions i and $i+2$ can be described by a logical OR relationship, modulated by potential interactions specific for the As*x* at position i, with residues at positions $i+4$ and $i+6$ adjacent to the turn. Furthermore, the results show that the thermodynamic contribution of the As*x* residues within such turns is substantial in comparison to the overall Gibbs energy of folding, such that mutational events within such turns are potentially catastrophic for protein stability and folding. The logical OR relationship between the As*x* residues in the As*x*-Pro-As*x*-Gly turn motif, however, can contribute redundancy that can negate the impact of such mutations. Such protective redundancy is demonstrated for the WT turn 6 DTDG sequence in FGF-1.

Results

Mutant protein purification

The majority of the mutant proteins behaved similarly to WT FGF-1 in the purification protocol; however, several turn 10 mutants exhibited reduced heparin-binding affinity due to mutation of Lys112 (at position i within turn 10), which contributes to the heparin-binding functionality of FGF-1.[16,17] These mutants were therefore purified by substituting gel filtration for heparin Sepharose affinity chromatography. The three double Ala mutations (APAG, turn 2; ATAG, turn 6; and AKAG, turn 10) exhibited extensive precipitation upon purification due to substantial destabilization. These mutations were therefore constructed within a more thermostable mutant form of FGF-1 containing Lys12Val and Pro134Val mutations.[18] This mutant form of FGF-1 is −19.1 kJ/mol more stable than WT FGF-1 (essentially doubling the stabilizing Gibbs energy), and the sites of mutation are distal to the turn 2, turn 6, and turn 10 regions. Within this background, each of the double Ala mutations yielded soluble natively folded protein. All mutant proteins were purified to apparent homogeneity on Coomassie-blue-stained SDS-PAGE with a yield of 30–60 mg/L.

Isothermal equilibrium denaturation

The thermodynamic parameters determined by isothermal equilibrium denaturation for the FGF-1 mutants are listed in Table 1. The standard error of ΔG from multiple analyses is approximately 1.0 kJ/mol (0.24 kcal/mol), which is also the typical magnitude of the standard deviation of the fit to the two-state model (data not shown). Thus, mutational effects on stability can be reliably measured for values >1.0 kJ/mol, consistent with previous reports.

When normalized against the appropriate double Ala reference protein, the stability effect for the introduction of an As*x* residue at position i is increased stability in each case, but the magnitude of the increase varies considerably (Fig. 2). Within turn 2, there is a differential effect between Asp and Asn, with Asn stabilizing the double Ala background by −7.6 kJ/mol and with Asp providing only a −3.0 kJ/mol increase in stability. In contrast, there is little differential effect between Asp and Asn at position i in turn 6 or turn 10; however, the introduction of an As*x* at position i in turn 6 stabilizes the protein by −15.1±0.3 kJ/mol, while the same As*x* mutation at position i in turn 10 stabilizes the protein by −9.1± 0.1 kJ/mol.

Table 1. Isothermal equilibrium denaturation data for As*x* mutations at positions *i* and *i*+2 within β-turns 2, 6, and 10 of FGF-1

Protein Mutant	Sequence	ΔG (kJ/mol)	*m*-value (kJ/mol M)	C_m (M)	$\Delta\Delta G^a$ (kJ/mol)	$\Delta\Delta G^b$ (kJ/mol)
WT*[c]		28.6±0.1	19.8± 0.1	1.45± 0.01		
K12V/P134V/C117V		37.6±0.6	18.5±0.3	2.03±0.01		
Turn 2	LPDG					
L26A/D28A[d]	APAG	26.4±0.9	20.3±0.7	1.30±0.01	14.2	0.00
D28A	LPAG	20.0±0.8	18.9±0.7	1.06±0.01	7.5	−6.6
L26D/D28A	DPAG	16.1±0.2	18.7±0.4	0.86±0.01	11.2	−2.8
L26N/D28A	NPAG	23.3±0.5	20.8±0.5	1.12±0.01	6.6	−7.5
L26A	APDG	25.9±0.8	20.2±0.6	1.28±0.01	3.2	−10.8
L26A/D28N	APNG	24.0±0.9	20.7±0.8	1.16±0.02	5.8	−8.3
L26D	DPDG	21.5±0.3	18.6±0.3	1.16±0.02	5.5	−8.6
L26D/D28N	DPNG	19.3±0.3	18.2±0.3	1.06±0.02	7.3	−6.8
L26N	NPDG	30.8±0.4	18.4±0.4	1.67±0.02	−4.4	−18.4
L26N/D28N	NPNG	29.0±0.6	19.3±0.3	1.50±0.01	−1.1	−15.1
Turn 6	DTDG					
D68A/D70A[d]	ATAG	21.8±0.6	17.8±0.4	1.23±0.01	14.7	0.00
D70A	DTAG	28.0±0.8	19.3±0.3	1.45±0.02	−0.1	−14.5
D68N/D70A	NTAG	27.0±0.1	18.2±0.1	1.48±0.01	−0.7	−15.1
D68A	ATDG	24.6±0.4	19.2±0.3	1.28±0.01	3.2	−11.2
D68A/D70N	ATNG	25.1±0.4	20.3±0.3	1.24±0.01	4.2	−10.3
WT[c]	DTDG	28.6±0.1	19.8±0.1	1.45±0.01	0.0	−14.5
D70N	DTNG	29.7±0.7	18.9±0.3	1.57±0.01	−2.5	−16.8
D68N	NTDG	28.4±0.3	18.6±0.1	1.53±0.01	−1.6	−16.1
D68N/D70N	NTNG	27.3±0.7	19.2±0.3	1.42±0.02	0.4	−13.9
Turn 10	KKNG					
K112A/N114A[d]	AKAG	26.5±0.6	17.4±0.3	1.52±0.01	9.1	0.0
N114A	KKAG	17.4±0.6	17.0±0.4	1.02±0.01	7.7	−1.2
K112D/N114A	DKAG	27.8±0.3	19.4±0.4	1.43±0.02	0.2	−8.8
K112N/N114A	NKAG	28.2±0.5	19.5±0.5	1.44±0.01	0.0	−9.0
K112A/N114D	AKDG	29.2±0.9	19.6±0.6	1.49±0.02	−0.9	−9.9
K112A	AKNG	30.0±0.9	19.9±0.6	1.50±0.02	−1.3	−10.1
K112D/N114D	DKDG	30.0±0.5	18.9±0.5	1.59±0.01	−2.8	−11.9
K112D	DKNG	30.7±0.4	18.4±0.1	1.67±0.01	−4.3	−13.4
K112N/N114D	NKDG	35.2±0.3	18.5±0.1	1.90±0.01	−8.8	−17.8
K112N	NKNG	33.9±0.6	19.0±0.6	1.78±0.02	−6.6	−15.6

[a] $\Delta\Delta G = (C_{m\ WT} - C_{m\ mutant})(m_{WT} + m_{mutant})/2$, as described by Pace and Scholtz.[19] WT* reference refers to the His93Gly mutant of FGF-1, except for double Ala mutations where the Lys12Val/Pro134Val/Cys117Val mutant of FGF-1 is the reference. A negative value of $\Delta\Delta G$ indicates a more stable mutation.
[b] Values calculated in reference to the Ala-*Xxx*-Ala-Gly mutant for that turn.
[c] All mutations, except double Ala, were constructed in the His93Gly mutant of FGF-1.[20]
[d] Double Ala mutations were constructed in the Lys12Val/Pro134Val/Cys117Val mutant of FGF-1.[18]

When normalized against the appropriate double Ala reference protein, the stability effects for the introduction of an As*x* residue at position *i*+2 within turns 2, 6, and 10 are notably consistent (Fig. 2). The introduction of an As*x* at position *i*+2 in turn 2 stabilizes the protein by −9.7±1.3 kJ/mol, of an As*x* at position *i*+2 in turn 6 stabilizes the protein by −11.0±0.5 kJ/mol, and of an As*x* at position *i*+2 in turn 10 stabilizes the protein by −10.2±0.2 kJ/mol.

The stability effects of the single As*x* point mutations at positions *i* and *i*+2 in turns 2, 6, and 10 are compared to the corresponding double mutants in Fig. 3. This comparison shows that the stability of a subset of the double As*x* mutations is essentially a simple sum of the stability contribution of the constituent point mutations, while other double As*x* mutations are nonadditive and less stable than expected for a simple sum. In turn 2, the NPNG and NPDG double mutants are essentially additive when compared to their constituent As*x* point mutants; however, the DPNG and DPDG double mutants are significantly less stable than the sum of their constituent point mutations. Furthermore, when considering the nonadditivity observed for the DPNG and DPDG double mutants, the stability of DPNG ($\Delta\Delta G$=−6.9 kJ/mol, in reference to the double Ala mutant) appears most similar to the APNG point mutant ($\Delta\Delta G$=−8.4 kJ/mol), and the stability of the DPDG double mutant ($\Delta\Delta G$=−8.7 kJ/mol, in reference to the double Ala mutant) appears most similar to the APDG point mutant ($\Delta\Delta G$=−11.0 kJ/mol). The turn 6 double As*x* mutants are substantially nonadditive and less stable than the sum of their constituent point mutations; however, their stability appears to reflect more closely the stability of the position *i* single As*x* mutation (thus, the NTNG double mutant stability is most similar to the NTAG single As*x* mutation, etc.). In turn 10, the NKNG and NKDG mutants are essentially additive in comparison to their constituent As*x* point mutations; however, the DKNG and DKDG double mutants exhibit significant nonadditivity (i.e., reduced stability) in comparison to the sum of their constituent single As*x* mutations. Since

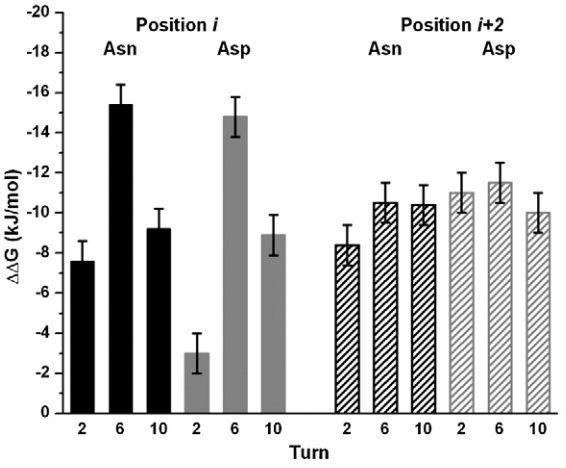

Fig. 2. The effects on stability of the introduction of As*x* point mutations at either position *i* (left panel) or position *i*+2 (right panel) in reference to the double Ala background (i.e., Ala-*Xxx*-Ala-Gly) at turns 2, 6, and 10 in FGF-1. Asn mutations are indicated in black, and Asp mutations are indicated in gray. Mutations at position *i* are indicated using filled columns, and mutations at position *i*+2 are indicated using hatched columns. The specific turn location is indicated by the *x*-axis label. $\Delta\Delta G$ values are taken from the isothermal equilibrium denaturation data, and negative values indicate increased stability.

the constituent single As*x* mutations for these double mutants (i.e., DKAG, AKNG, and AKDG) exhibit near-identical $\Delta\Delta G$ values, it is not clear from the stability data alone which single As*x* mutant is most similar in stability to the DKNG and DKDG double mutants.

Folding and unfolding kinetics

A summary of the folding and unfolding kinetics values is given in Table 2. A comparison of the $\Delta\Delta G$ values determined from the folding and unfolding kinetics data with those determined from the isothermal equilibrium data is given in Fig. 4. Overall, there is excellent agreement between the two methods; therefore, the stability effects of the mutations can be interpreted in terms of the differential effects on folding and unfolding kinetics.

The effects of the As*x* mutations on $\Delta\Delta G_f$ and $\Delta\Delta G_u$ (calculated in reference to the Ala-*Xxx*-Ala-Gly background) are shown in Fig. 5. In turn 2, the introduction of As*x* residues at positions *i* and *i*+2 serves to increase the folding rate constant, with essentially no effect on the unfolding rate constant. The double As*x* mutations NPNG and NPDG (i.e., those with Asn at position *i*) are essentially additive in terms of the energetic effects associated with increases in the folding rate constant. In contrast, the double As*x* mutations DPNG and DPDG (i.e., those with Asp at position *i*) are nonadditive in comparison to their respective point mutations; their folding behavior is more like the constituent APNG and APDG point mutants.

In turn 6, the introduction of As*x* mutations at positions *i* and *i*+2 is associated, in all cases, with both an increase in the folding rate constant and a decrease in the unfolding rate constant. The double As*x* mutations are nonadditive and, in each case,

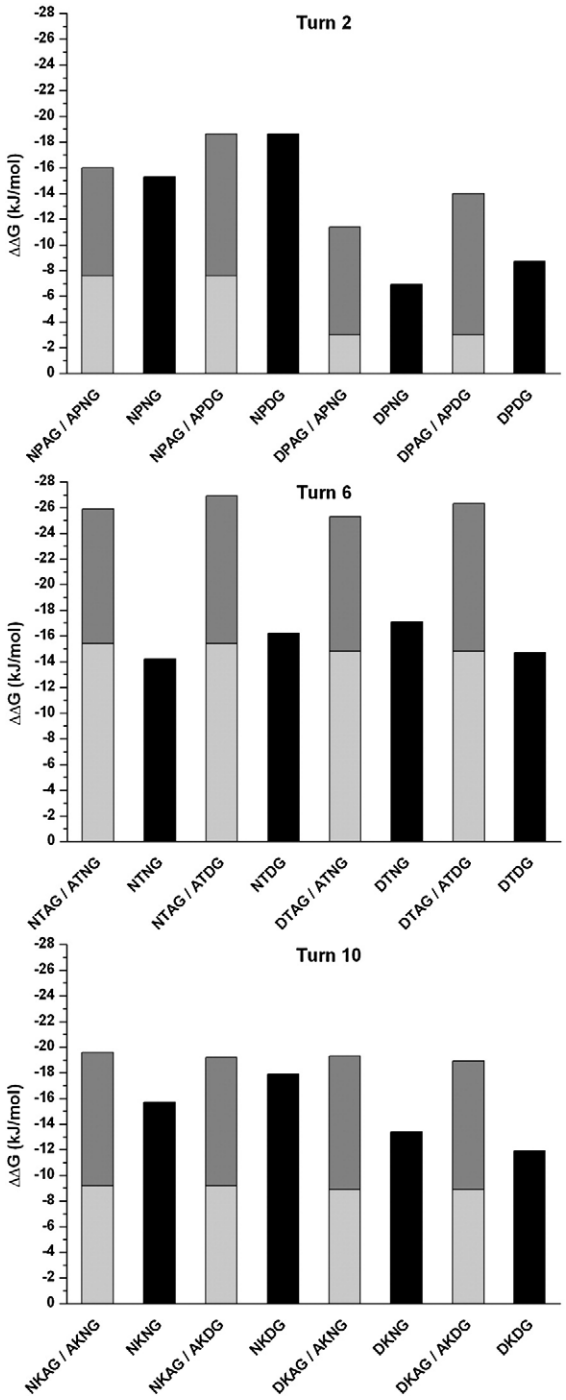

Fig. 3. Stability data (in reference to Ala-*Xxx*-Ala-Gly background) for single As*x* mutations at position *i* (light gray) and position *i*+2 (dark gray) in turns 2, 6, and 10 (summation of point mutations as stacked columns), and experimental values for corresponding double As*x* mutants (black). $\Delta\Delta G$ values are taken from the isothermal equilibrium denaturation data, and negative values indicate increased stability.

Table 2. Folding and unfolding kinetics parameters for WT and mutant FGF-1 proteins

Protein Mutant	Sequence	k_f (s^{-1})	m_f (kJ/mol M)	k_u (1×10^{-3} s^{-1})	m_u (kJ/mol M)	m-value (kJ/mol M)	C_m (M)	$\Delta\Delta G$[a] (kJ/mol)	$\Delta\Delta G_u$ (kJ/mol)	$\Delta\Delta G_f$ (kJ/mol)	$\Delta\Delta G$[b] (kJ/mol)	$\Delta\Delta G_f$[b] (kJ/mol)	$\Delta\Delta G_u$[b] (kJ/mol)	ϕ_f	ϕ_u
WT*[c]		55.1	−18.4	0.44	1.2	19.6	1.49								
K12V/P134V/C117V		125	−15.0	0.09	2.1	17.2	2.04								
Turn 2	LPDG														
L26A/D28A[d]	APAG	2.06	−16.6	0.18	1.6	18.2	1.28	13.6	−0.8	12.8	0.0	0.0	0.0		
D28A	LPAG	1.42	−15.5	0.35	1.3	16.8	1.23	4.7	0.4	5.1	−8.9	−7.7	1.2	1.05	−0.07
L26D/D28A	DPAG	1.35	−17.6	0.77	1.0	18.6	1.00	9.3	−1.2	8.2	−4.2	−4.6	−0.4	0.74	0.11
L26N/D28A	NPAG	3.52	−17.5	0.36	1.3	18.8	1.21	5.2	0.3	5.5	−8.4	−7.3	1.1	1.29	−0.09
L26A	APDG	18.3	−19.2	0.52	1.1	20.3	1.28	4.1	−0.3	3.8	−9.5	−9.0	0.5	1.01	0.15
L26A/D28N	APNG	2.89	−17.6	0.50	1.1	18.7	1.15	6.4	−0.2	6.2	−7.2	−6.5	0.6	1.59	0.07
L26D	DPDG	6.90	−17.2	0.89	1.0	18.2	1.22	5.0	−1.5	3.5	−8.6	−9.3	−0.7		
L26D/D28N	DPNG	4.19	−16.8	0.84	1.1	17.9	1.18	5.7	−1.5	4.2	−7.9	−8.6	−0.7		
L26N	NPDG	66.4	−16.7	0.36	1.3	18.0	1.67	−3.4	0.2	−3.2	−17.0	−16.0	1.0		
L26N/D28N	NPNG	27.9	−17.3	0.36	1.3	18.5	1.50	−0.4	0.3	−0.1	−14.0	−12.8	1.1		
Turn 6	DTDG														
D68A/D70A[d]	ATAG	0.15	−8.3	0.77	2.7	11.0	1.19	12.0	−6.2	5.8	0.0	0.0	0.0		
D70A	DTAG	33.9	−17.8	0.51	1.0	18.8	1.47	0.4	−0.1	0.3	−11.6	−5.6	6.1		
D68N/D70A	NTAG	52.2	−17.2	0.61	1.3	18.4	1.53	−0.8	−1.0	−1.7	−12.8	−7.6	5.2		
D68A	ATDG	17.9	−17.2	1.09	1.5	18.7	1.29	3.8	−2.7	1.1	−8.3	−4.8	3.5	0.33	0.85
D68A/D70N	ATNG	21.8	−17.3	1.29	1.4	18.7	1.29	3.8	−3.0	0.8	−8.3	−5.1	3.2	0.19	0.71
WT[c]	DTDG	55.1	−18.4	0.44	1.2	19.6	1.49	0.0	0.0	0.0	−12.0	−5.8	6.2		
D70N	DTNG	71.9	−17.0	0.61	1.1	18.1	1.60	−2.1	−0.7	−2.8	−14.1	−8.7	5.5		
D68N	NTDG	71.2	−17.0	0.71	1.3	18.3	1.56	−1.4	−1.4	−2.8	−13.4	−8.6	4.8		
D68N/D70N	NTNG	33.6	−16.9	0.79	1.2	18.1	1.46	0.6	−1.5	−1.0	−11.5	−6.8	4.6		
Turn 10	KKNG														
K112A/N114A[d]	AKAG	27.0	−12.5	0.72	4.0	16.5	1.58	7.8	−8.6	−0.7	0.0	0.0	0.0		
N114A	KKAG	6.23	−12.2	9.39	2.2	14.4	1.12	6.2	−8.9	−2.7	−1.6	−1.9	−0.3	−0.35	1.15
K112D/N114A	DKAG	51.7	−15.7	1.26	1.4	17.1	1.54	−0.9	−3.0	−3.9	−8.7	−3.1	5.6		
K112N/N114A	NKAG	60.3	−16.0	1.71	1.3	17.3	1.50	−0.2	−3.6	−3.8	−8.1	−3.0	5.0		
K112A/N114D	AKDG	39.9	−17.2	0.40	1.0	18.3	1.56	−1.4	0.4	−1.0	−9.3	−0.3	9.0		
K112A	AKNG	40.9	−16.4	1.01	1.2	17.6	1.49	−0.2	−2.1	−2.2	−8.0	−1.5	6.5		
K112D/N114D	DKDG	42.2	−16.0	0.49	1.2	17.2	1.64	−2.8	−0.3	−3.1	−10.6	−2.4	8.2		
K112D	DKNG	92.0	−17.3	0.70	1.0	18.3	1.60	−2.1	−1.0	−3.1	−9.9	−2.3	7.6		
K112N/N114D	NKDG	93.0	−17.4	0.09	0.9	18.3	1.87	−7.4	4.4	−3.1	−15.3	−2.3	13.0		
K112N	NKNG	47.5	−15.2	0.26	1.1	16.3	1.84	−6.4	1.5	−4.9	−14.2	−4.2	10.0		

[a] $\Delta\Delta G=(C_{m\ WT}-C_{m\ mutant})(m_{WT}+m_{mutant})/2$, as described by Pace and Scholtz.[19] WT* reference refers to the His93Gly mutant of FGF-1, except for double Ala mutations where the Lys12Val/Pro134Val/Cys117Val mutant of FGF-1 is the reference. A negative value of $\Delta\Delta G$ indicates a more stable mutation.
[b] Values calculated in reference to the Ala-*Xxx*-Ala-Gly mutant for that turn.
[c] All mutations, except double Ala, were constructed in the His93Gly mutant of FGF-1.[20]
[d] Double Ala mutations were constructed in the Lys12Val/Pro134Val/Cys117Val mutant of FGF-1.[18]

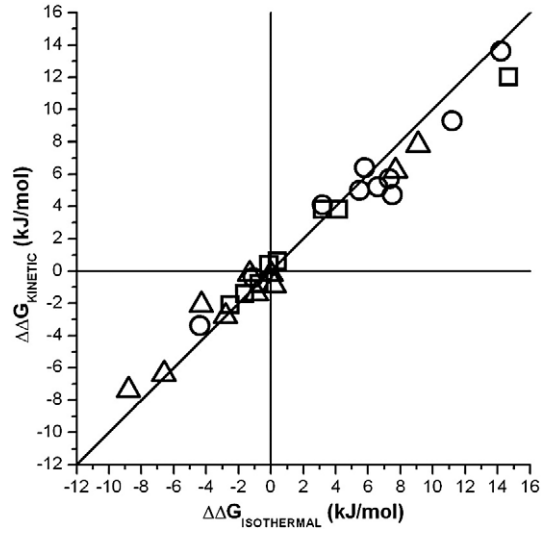

Fig. 4. A comparison of the $\Delta\Delta G$ values from isothermal equilibrium and folding kinetics data in reference to the WT* protein for turn 2 (circles), turn 6 (squares), and turn 10 (triangles) mutants. Negative values for $\Delta\Delta G$ indicate increased stability.

closely resemble the folding and unfolding kinetics behavior of the constituent point mutation at position *i*.

In turn 10, the introduction of As*x* mutations at positions *i* and *i*+2, in each case, is associated primarily with a decrease in the unfolding rate constant, with only a minimal increase in the folding rate constant. For the NKNG and NKDG double As*x* mutations (i.e., where position *i* is an Asn), the energetic effects associated with changes in both folding and unfolding rate constants are essentially additive. For the DKNG and DKDG double As*x* mutations, the effects are nonadditive in comparison to the constituent point mutations.

X-ray structures

Diffraction quality crystals were obtained for a total of 12 mutant proteins, and high-resolution (2.00–1.50 Å) data sets were collected in each case. Mutant structures refined to excellent crystallographic residual and stereochemistry (Table 3). Details of the individual crystal, diffraction data set, and refinement statistics are provided in Supplementary Tables 1–3. The X-ray structure of the WT protein has previously been reported,[21] and this provides structural details of the WT turn 2 (LPDG), turn 6 (DTDG), and turn 10 (KKNG) regions. Turn 6 is located near a crystal contact in the WT space group $C222_1$ [see Protein Data Bank (PDB) accession number 1JQZ], and mutations in this turn proved difficult to crystallize. One mutant in turn 6 (D70A) did yield diffraction quality crystals, but crystallized in a different space group (space group $P2_1$; see Supplementary Table 3). Thus, structural data for mutations in turn 6 are limited, presumably due to crystal contact effects.

Discussion

A comparison of the NPAG (turn 2), DPAG (turn 2), DTAG (turn 6), and NKAG (turn 10) structures provides information regarding the preferred rota-

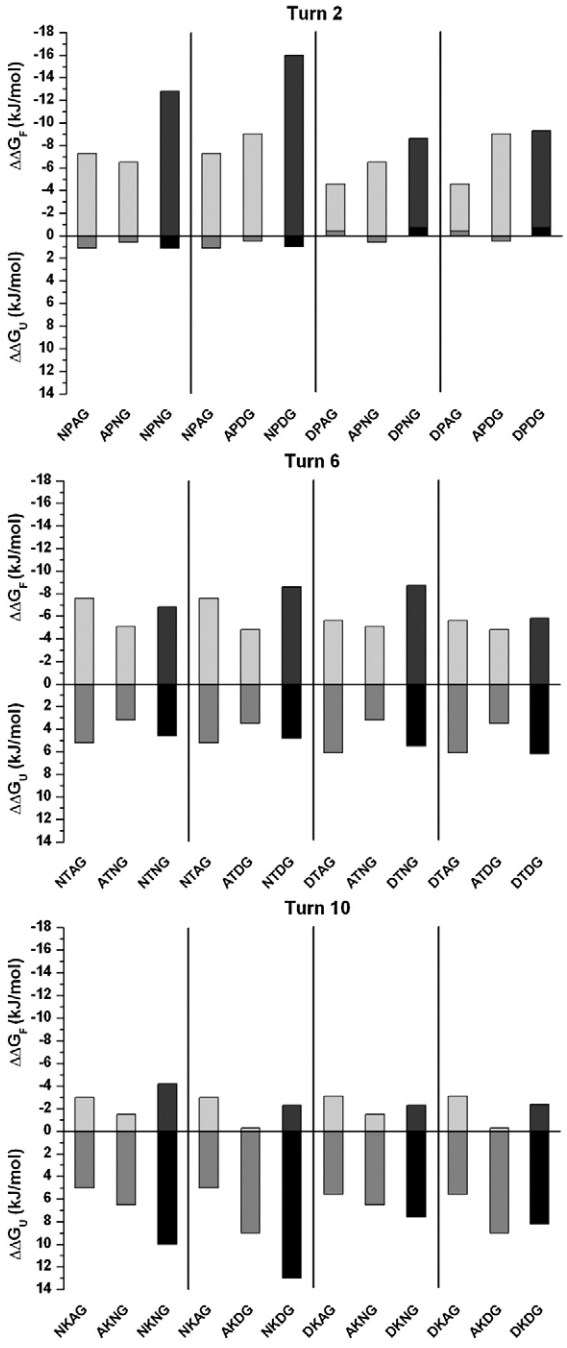

Fig. 5. Differential effects on $\Delta\Delta G_f$ and $\Delta\Delta G_u$ values for single and double As*x* mutants at turns 2, 6, and 10, in reference to the double Ala mutant background (Ala-*Xxx*-Ala-Gly). Light gray bars show the effects on $\Delta\Delta G_f$ for single As*x* mutations; gray bars show the effects on $\Delta\Delta G_u$ for single As*x* mutations; dark gray bars show the effects on $\Delta\Delta G_f$ for double As*x* mutations; and black bars show the effects on $\Delta\Delta G_u$ for double As*x* mutations. A negative value for $\Delta\Delta G_f$ and a positive value for $\Delta\Delta G_u$ contribute to stabilization (i.e., $\Delta\Delta G = \Delta\Delta G_f - \Delta\Delta G_u$).

Table 3. Summary of X-ray structure data for As*x* mutants at positions *i* and *i*+2 in turns 2, 6, and 10 of FGF-1

Mutation	Turn sequence	Resolution (Å)	R_{cryst} (%)	R_{free} (%)	PDB accession code
Turn 2					
WT[a]	LPDG				
Leu26Asn	NPDG	1.55	19.4	21.1	3BAO
Asp28Ala	LPAG	1.75	19.5	23.2	3BA5
Leu26Asn/ Asp28Ala	NPAG	1.60	19.5	22.5	3BA7
Leu26Ala	APDG	1.80	19.3	21.6	3BAQ
Leu26Asp/ Asp28Ala	DPAG	1.60	20.5	23.3	3BAU
Leu26Ala/ Asp28Asn	APNG	1.62	19.3	21.8	3BAV
Leu26Asn/ Asp28Asn	NPNG	1.55	19.1	20.0	3B9U
Leu26Asp/ Asp28Asn	DPNG	1.50	19.8	22.8	3BB2
Leu26Asp	DPDG	1.80	18.9	21.9	3BA4
Turn 6					
WT[a]	DTDG				
Asp70Ala	DTAG	2.00	21.3	25.3	3BAD
Turn 10					
WT[a]	KKNG				
Lys112Asn/ Asn114Ala	NKAG	1.75	19.4	22.4	3BAG
Lys112Asn	NKNG	1.65	18.7	20.5	3BAH

[a] PDB accession code 1JQZ.[21]

mer orientation of an As*x* residue at position *i* when position *i*+2 is occupied by an Ala. With the exception of the NPAG (turn 2) structure, in each case, the As*x* at position *i* adopts a *gauche*$^-$ rotamer and H-bonds with the main-chain amide of turn residues *i*+2 and *i*+4 (Fig. 6a). Conversely, the Asn in the NPAG (turn 2) structure adopts a *gauche*$^+$ rotamer and H-bonds with the *i*+6 Asp side chain (with solvent providing the H-bond partner for the main-chain amide at position *i*+2, and no obvious H-bond partner for the *i*+4 main-chain amide). Furthermore, turn 2 appears unique in that deletion of the WT Leu side chain (by mutation to Ala) at position *i* is associated with 3.2 kJ/mol of destabilization (in contrast, the Ala substitution of the WT Lys residue at position *i* in turn 10 is essentially neutral; Table 1). The Leu at position *i* in this turn adopts a *gauche*$^+$ rotamer (like the Asn point mutant) and makes extensive van der Waals contacts with the aliphatic chain of the adjacent *i*−2 Arg (see Fig. 6b). These adjacent H-bond and van der Waals interactions appear to stabilize the Asn side chain in the NPAG turn 2 sequence in the atypical *gauche*$^+$ rotamer. Since an Asp cannot participate as an H-bond donor, and also due to potential charge repulsion, an Asp at position *i* will not be similarly stabilized in the *gauche*$^+$ rotamer. The structural data therefore provide a rationale for the atypical *gauche*$^+$ Asn rotamer and for the Asp/Asn stability differential favoring Asn at position *i* in turn 2.

A comparison of the LPDG (turn 2), APDG (turn 2), APNG (turn 2), and KKNG (turn 10) structures (Fig. 6b) provides details of the preferred rotamer orientation of an As*x* residue at position *i*+2 when position *i* is occupied by an Ala (or non-As*x* residue as in the LPDG and KKNG structures). In each case, the As*x* at position *i*+2 adopts a *gauche*$^-$ rotamer and H-bonds with the main-chain amide of turn residue *i*+4. The solvent provides the H-bond partner for the main-chain amide at the turn position *i*+2. Overall, therefore, the structural data show that individual As*x* residues at both positions *i* and *i*+2 in type I β-turns exhibit a preferred *gauche*$^-$ rotamer that provides H-bond acceptor interactions for specific main-chain amides within the turn and forms the basis for the observed −10- to −15-kJ/mol increase in stability in reference to Ala.

A key question is related to the simultaneous presence of As*x* residues at positions *i* and *i*+2, since both residues cannot simultaneously adopt the preferred *gauche*$^-$ rotamer due to steric contact between them (e.g., compare Fig. 6a and b). In the absence of local interactions, the stability data suggest that the As*x* at position *i* is likely to be "dominant" to that at *i*+2 due to its participation in two main-chain amide H-bonds (with turn amides *i*+2 and *i*+4), as compared to a single interaction for an As*x* at position *i*+2 (with amide *i*+4). Furthermore, if these stabilizing interactions are mutually exclusive, then the stability effects should be nonadditive and primarily reflect the contribution of the dominant As*x* residue (whether it be at position *i* or position *i*+2).

As noted above, an exception to the preferred *gauche*$^-$ rotamer was seen in the X-ray structure of the NPAG turn 2 mutant (Fig. 6a). A comparison of the NPAG, APDG, and NPDG double mutants shows that the structural details of the NPDG double mutant are a composite of those of the individual NPAG and APDG point mutants (Fig. 7a). The *gauche*$^+$ rotamer of the Asn at position *i* and the *gauche*$^-$ rotamer of the Asp at position *i*+2 are compatible, since no steric hindrance exists between them. The stability and folding effects are likewise essentially additive (Tables 1 and 2; Figs. 3 and 5). A comparison of the X-ray structure of the NPNG double mutant with those of the NPAG and APNG single mutants is essentially an identical analysis, as are the additive effects on stability and folding (Tables 1 and 2; Figs. 3 and 5).

The DPAG, APDG, and DPDG X-ray structures (Fig. 7b) permit comparison of individual and combined Asp mutations at positions *i* and *i*+2 for a combination that is nonadditive in stability effects (Tables 1 and 2; Figs. 3 and 5). Both of the single Asp mutants adopt the preferred *gauche*$^-$ rotamer. In the double Asp mutant, the Asp at position *i* changes to a *trans* rotamer, and the *gauche*$^-$ rotamer of the *i*+2 Asp is retained; thus, in this case, the Asp at position *i*+2 is dominant. The stability and folding kinetics data also indicate that the DPDG double mutant principally inherits the properties of the APDG single mutant (Figs. 3 and 5). Although the Asp at position *i* can participate in two main-chain H-bond interactions when in the *gauche*$^-$ rotamer, the X-ray structure shows that the Thr side chain at position

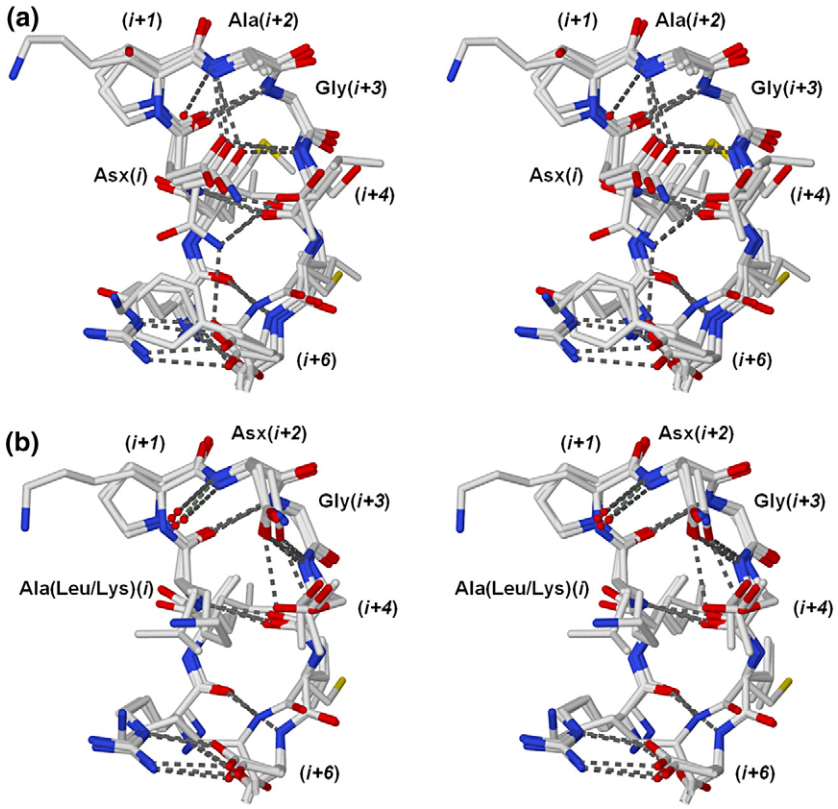

Fig. 6. (a) Overlay of mutant X-ray structures NPAG (turn 2), DPAG (turn 2), DTAG (turn 6), and NKAG (turn 10) mutant structures. These structures evaluate the orientation of Asx at position *i* when position *i*+2 is Ala. With the exception of the NPAG structure, in each case, the Asx at position *i* adopts a *gauche*$^-$ rotamer and H-bonds with the main-chain amide of turn residues *i*+2 and *i*+4. The Asn in the NPAG structure adopts a *gauche*$^+$ rotamer and H-bonds with the *i*+6 Asp side chain. (b) Overlay of mutant X-ray structures APDG (turn 2), APNG (turn 2), KKNG (turn 10), and WT turn 2 structure LPDG. These structures evaluate the orientation of Asx at position *i*+2 when position *i* is Ala (or non-Asx as in the KKNG and LPDG structures). In each case, the Asx at position *i*+2 adopts a *gauche*$^-$ rotamer and H-bonds with the main-chain amide of turn residue *i*+4. The solvent provides the H-bond partner for the main-chain amide at the turn position *i*+2.

i+4 rotates to H-bond with the Asp at position *i*+2. Thus, interactions with the adjacent *i*+4 Thr residue contribute to make the *i*+2 Asp dominant in this turn. The DPAG, APNG, and DPNG mutant structures permit a similar analysis when position *i*+2 is Asn instead of Asp. Analysis of these structures indicates an identical result as with the APDG structure (data not shown), and the stability and folding data exhibit similar behaviors as seen with the APDG mutant.

A comparison of DTAG, ATDG, and DTDG X-ray structures permits a similar evaluation for dual Asp mutations in turn 6. X-ray structures are available for the DTAG and DTDG turn sequences, but a structure for the ATDG mutant was not obtained. However, based upon available Ala-*Xxx*-Asx-Gly X-ray structures, a *gauche*$^-$ rotamer for the *i*+2 Asx is presumably adopted. In the DTAG single Asp X-ray structure, the Asp at position *i* adopts the preferred *gauche*$^-$ rotamer and participates as an H-bond acceptor for the main-chain amides at positions *i*+2 and *i*+4 (Fig. 7c). In the DTDG double Asp X-ray structure, the *gauche*$^-$ rotamer of the Asp at position *i* is retained, and the Asp at *i*+2 adopts a *gauche*$^+$ rotamer; thus, in this turn, the Asp at position *i* is dominant. In contrast to turn 2, the turn 6 sequence does not have a Thr (or Ser) at position *i*+4; therefore, an additional H-bond with the Asp at position *i*+2 (in the *gauche*$^-$ rotamer) is not possible. This provides a structural rationale for the dominance of the *i* Asp in turn 6. The stability and folding data show that the DTDG double Asp mutant inherits the stability and folding properties of the DTAG single Asp mutant (Figs. 3 and 5), in agreement with the available X-ray structure data showing that the dominant Asp is at position *i*. Although additional structural data are not available for other mutations in turn 6, the stability and folding data are consistent with the position *i* Asx dominance in each case (Figs. 3 and 5).

The NKAG and NKNG X-ray structures permit a comparison of the effects of combining Asn mutations at positions *i* and *i*+2 in turn 10. As previously detailed, the single Asn mutant at position *i* in the NKAG structure adopts the preferred *gauche*$^-$ rotamer and provides H-bond acceptors to the main-chain amides at positions *i*+2 and *i*+4 (Fig. 7d). Although a structure for the AKNG mutant was not determined, all available data indicate that the Asn at position *i*+2 likely adopts the preferred *gauche*$^-$ rotamer. In the NKNG double Asn mutant, the *i*+2 Asn adopts the preferred *gauche*$^-$ rotamer, but the Asn at position *i* shifts from *gauche*$^-$ to *gauche*$^+$. However, in the *gauche*$^+$ rotamer, the Asn at position *i* provides an H-bond donor to the Ser at position *i*+4, which in turn adopts an alternate rotamer (*gauche*$^-$) to participate in this interaction. Additionally, in the *gauche*$^+$ rotamer, the Asn at position *i* provides an H-bond acceptor to the Lys side chain at position *i*+6 in the turn. Finally, with the Asn at position *i* adopting the *gauche*$^+$ rotamer, the solvent provides the H-bond acceptor to the main-chain amide at position *i*+2 (thus, both *i*+2 and *i*+4 main-chain amide H-bond requirements are maintained). The stability and folding of both the NKNG and the NKDG double mutants are largely additive in na-

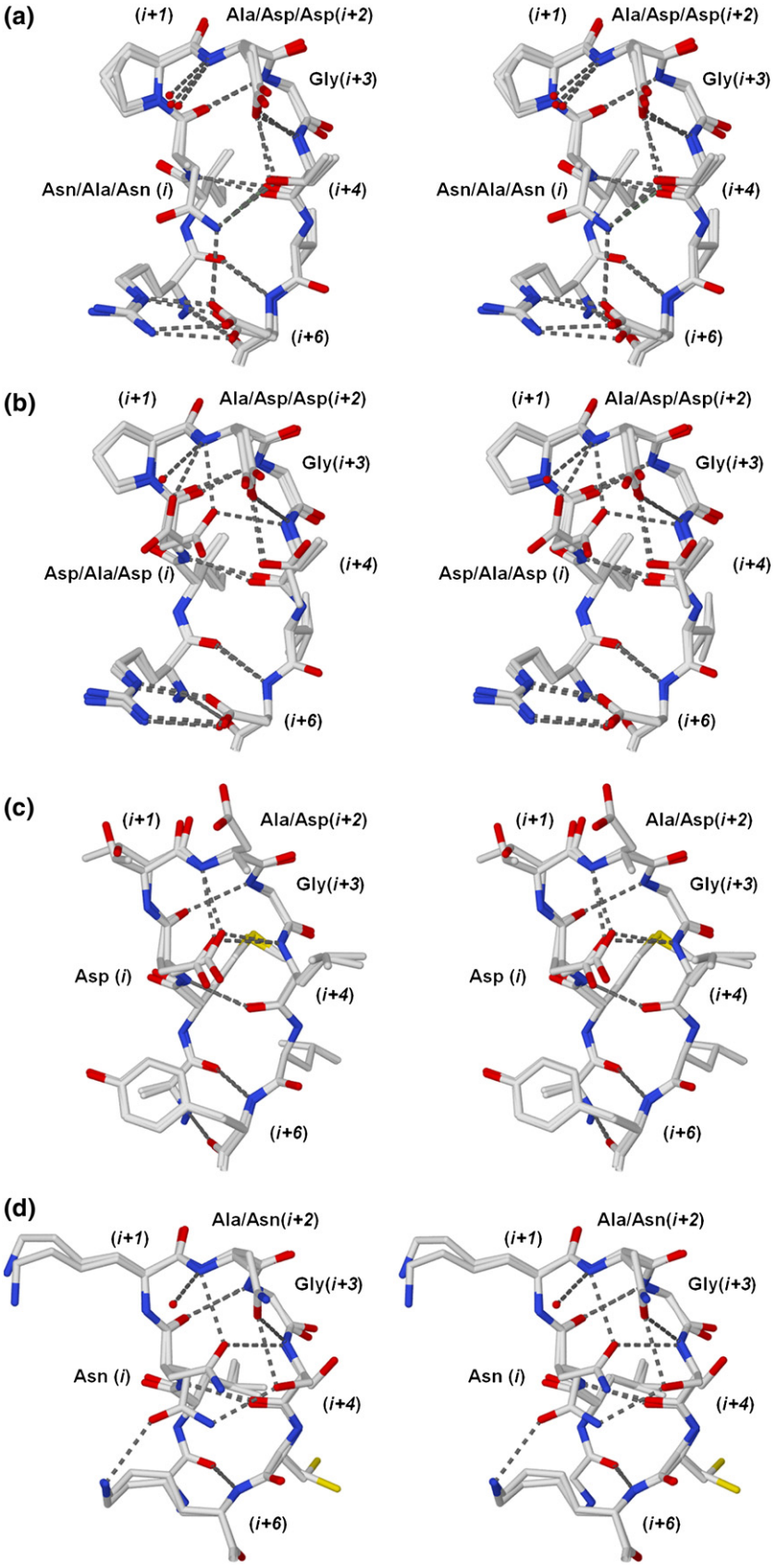

Fig. 7. (a) Overlay of mutant NPAG, APDG, and NPDG (turn 2) X-ray structures. These structures evaluate the orientation of the double As*x* mutant in comparison to the corresponding single As*x* mutations. In the double As*x* mutant, the *gauche*$^+$ rotamer of the *i* Asn and the *gauche*$^-$ rotamer of the *i*+2 Asp are retained. Both the structural and the stability effects of the individual Ala mutations are also observed to be additive. (b) Overlay of mutant X-ray structures DPAG, APDG, and DPDG (turn 2). These structures evaluate the orientation of the double Asp mutant at positions *i* and *i*+2 in comparison to the corresponding single Asp mutations. As single Asp mutants, both Asp residues adopt the *gauche*$^-$ rotamer; however, these are mutually exclusive due to steric contact. In the double Asp mutant, the Asp at position *i* adopts a *trans* rotamer, and the *gauche*$^-$ rotamer of the *i*+2 Asp is retained. (c) Overlay of mutant DTAG and WT DTDG (turn 6) X-ray structures. These structures evaluate the orientation of the double Asp mutant at positions *i* and *i*+2 in comparison to the corresponding single Asp mutation at position *i*. In the double Asp mutant, the *gauche*$^-$ rotamer of the *i* Asp is retained, and the Asp at *i*+2 adopts a *gauche*$^+$ rotamer. (d) Overlay of mutant NKAG and NKNG (turn 10) X-ray structures. In the double Asn mutant, the *gauche*$^-$ rotamer of the *i*+2 Asn is retained, but the Asn at position *i* shifts from preferred *gauche*$^-$ to *gauche*$^+$. However, in the *gauche*$^+$ rotamer, the Asn at position *i* provides an H-bond donor to the Ser at position *i*+4, which adopts an alternate rotamer to participate in this interaction. The stability and folding of both the NKNG and the NKDG double mutants are largely additive in nature; thus, the alternate rotamer of Asn *i* may be energetically similar to the preferred *gauche*$^-$ interaction.

ture; thus, the alternate *gauche*$^+$ rotamer adopted by *i* Asn in the double As*x* mutant may be energetically similar to the preferred *gauche*$^-$ interaction observed in the single Asn mutant.

The results identify a complex interplay between the As*x* residues in the statistically preferred As*x*-Pro-As*x*-Gly motif in type I β-turns. Individual As*x* residues at positions *i* and *i*+2 are able to satisfy the

H-bonding requirement of the main-chain amide at position $i+4$. Furthermore, if the As*x* is at position i, it can simultaneously satisfy the H-bond requirement of the main-chain amide at position $i+2$ (if the As*x* is instead located at position $i+2$, then the solvent provides the H-bond partner for the $i+2$ main-chain amide). The main-chain amides require an H-bond acceptor as a partner; therefore, either Asp or Asn can fulfill this role. The stabilization free energy associated with the As*x*/main-chain amide H-bond appears substantial: as much as −15 kJ/mol provided by the As*x* at position i and −10 kJ/mol provided by the As*x* at position $i+2$. However, in the absence of interactions with the local turn environment, the As*x* residues at positions i and $i+2$ participate in a "logical OR" relationship. The preferred *gauche*$^-$ rotamer for As*x* residues to participate in main-chain amide H-bond interactions positions i and $i+2$ is mutually exclusive due to steric considerations. Therefore, if both As*x* residues are present in the turn sequence, one of them is dominant and provides the main-chain H-bond to the $i+4$ amide. The other As*x* must adopt an alternative rotamer (either *trans* or *gauche*$^+$). If the As*x* at position $i+2$ adopts an alternate *trans* or *gauche*$^+$ rotamer, it orients towards the solvent, and the stability and folding effects for the double As*x* sequence are essentially identical with those of the single As*x* mutant at position *i*. However, if the As*x* at position i adopts a *gauche*$^+$ rotamer, it has the possibility of H-bonding with amino acid side chains at residue positions $i+4$ (e.g., Thr or Ser) and $i+6$ (e.g., Asp or Lys) within the turn, and these interactions can modulate the stability effects such that stability and folding contributions of both i and $i+2$ As*x* residues in the turn can become additive. If the As*x* at position i adopts a *trans* rotamer, it can H-bond with the main-chain amide at position $i+2$, but it loses its interaction with the main-chain amide at position $i+4$. This may involve some strain and may not provide optimal H-bond interactions or stability.

As described above, the energetic contribution of As*x* residues in the β-turn is shown to be substantial. The Gibbs energy of unfolding for FGF-1, for example, is 21.1 kJ/mol; thus, the mutational loss of an As*x* within any one of the 11 β-turns in the structure could be catastrophic to the foldability of the protein. However, the logical OR relationship of the As*x* residues provides potential redundancy, such that the mutational loss of a single As*x* residue can be compensated for by the second. The primary structure of turn 6 in FGF-1 (DTDG) is unique in having As*x* residues at both positions i and $i+2$, and a thermodynamic cycle involving single Ala mutations demonstrates the logical OR redundancy present within the turn that can protect the protein from such mutations (Fig. 8).

The results highlight both the magnitude and the complexity of β-turn structure in contributing to a foldable polypeptide, and also the difficulty in elucidating the basis of the statistically preferred sequences comprising such turns. For example, the logical OR relationship between As*x* residues means

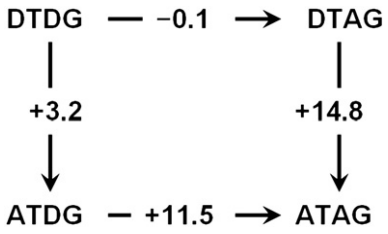

Fig. 8. Thermodynamic cycle for Ala mutations in the WT FGF-1 turn 6 (DTDG) structure that illustrates the logical OR relationship of the As*x* residues that provides for redundancy in stability.

that mutational analyses will produce substantially different results depending upon whether one or both As*x* residues are present. Furthermore, the results show that a complete understanding of the stability effects associated with the β-turn sequence requires knowledge of potential interactions with residues adjacent to the turn (especially $i+4$ and $i+6$).

A completely unexpected result from the present report is that although the three turns being studied are related by the 3-fold structural symmetry of the β-trefoil architecture (Fig. 1), the kinetics data indicate that they have dramatically different properties as regard contribution to the folding transition state structure. ϕ value analysis can be applied for Ala point mutations and where $\Delta\Delta G$ values are significantly above the standard deviation.[22,23] In comparison to the WT* protein, ϕ values can therefore be determined for the LPAG, DPAG, NPAG, APDG, and APNG mutants in turn 2, the ATDG and ATNG mutants in turn 6, and the KKAG mutant in turn 10. These ϕ values suggest that positions i and $i+2$ in turn 2 are as folded in the transition state as they are in the native state. The analysis is limited for mutations in turns 6 and 10; however, the data suggest that position $i+2$ in turn 10 is as unstructured in the transition state as it is in the denatured state, and position i in turn 6 falls midway between these two extremes, indicating that this position in turn 6 is partially structured in the transition state or that there are different folding pathways—some where this position is structured in the transition state and others where it is unstructured. A comparative analysis of the $\Delta\Delta G_u$ and $\Delta\Delta G_f$ values for all mutants (Fig. 5) is entirely consistent with the ϕ value analysis for both positions i and $i+2$ in each turn and indicates that turn 2 is structured in the transition state, turn 10 is unstructured, and turn 6 is partially structured (or there are multiple folding pathways where it is either structured or unstructured) in the transition state. Thus, despite the symmetric relationship in the tertiary structure, these turns make uniquely different contributions to the transition state structure in the folding pathway. This property suggests that the local turn sequence, while a primary determinant of stability, is not the primary determinant of turn structure in the folding transition state.

Materials and Methods

Mutagenesis and expression

Mutant construction and expression followed previously described procedures.[21,24,25] Briefly, all studies utilized a synthetic gene for the 140-amino-acid form of human FGF-1,[15,26–28] with the addition of an amino-terminal six residue "His-tag" to facilitate purification.[21] WT FGF-1 exhibits a characteristically low thermal stability.[24,29] In the present study, a His93Gly mutant form of FGF-1 was chosen as a stabilizing background protein for biophysical studies and is referred to herein as WT*. The His93Gly mutation provides an additional −6.6 kJ/mol of stability in comparison to WT FGF-1,[20] therefore permitting moderately destabilizing mutations to be isolated and characterized. For purposes of crystal growth, His93Gly, Lys12Val, and WT FGF-1 were used as the background proteins (depending upon crystal screening results). The His93Gly and Lys12Val mutations in the FGF-1 structure are distal to the turn locations being studied.

The QuikChange™ site-directed mutagenesis protocol (Stratagene, La Jolla, CA) was used to introduce individual or combination mutations using mutagenic oligonucleotides of 25–31 bases in length (Biomolecular Analysis Synthesis and Sequencing Laboratory, Florida State University). All FGF-1 mutants were expressed using the pET21a(+) plasmid/BL21(DE3) *Escherichia coli* host expression system (Invitrogen Corp., Carlsbad, CA). Mutant proteins were purified as previously described[21] using nickel-nitrilotriacetic acid chromatography followed by affinity purification using heparin Sepharose chromatography (GE Healthcare, Piscataway, NJ).

Isothermal equilibrium denaturation

Isothermal equilibrium denaturation by guanidine HCl (GuHCl) was quantified using fluorescence as the spectroscopic probe. FGF-1 contains a single buried tryptophan residue (Trp107) that exhibits greater fluorescence quenching in the native state *versus* the denatured state.[15,24] The differential fluorescence between the native state and the denatured state has been used to quantify the unfolding of FGF-1, in excellent agreement with unfolding as monitored by CD spectroscopy.[24,30] Fluorescence data were collected on a Varian Eclipse fluorescence spectrophotometer equipped with a Peltier controlled-temperature regulator at 298 K and using a 1-cm path-length cuvette. Protein samples (5 μM) were equilibrated overnight in 20 mM *N*-(2-acetamido)iminodiacetic acid (ADA), 100 mM NaCl, and 2 mM DTT (pH 6.6) ("ADA buffer") at 298 K in 0.1 M increments of GuHCl. Triplicate scans were collected and averaged, and buffer traces were collected and subsequently subtracted from the protein scans. All scans were integrated to quantify the total fluorescence as a function of denaturant concentration. The general purpose nonlinear least squares fitting program DataFit (Oakdale Engineering, Oakdale, PA) was used to fit the change in fluorescence *versus* GuHCl concentration data to a six-parameter two-state model:[31]

$$F = \frac{F_{0N} + S_N[D] + (F_{0D} + (S_D[D]))e^{-(\Delta G_0 + m[D])/RT}}{1 + e^{-(\Delta G_0 + m[D])/RT}} \quad (1)$$

where [D] is the denaturant concentration; F_{0N} and F_{0D} are the 0-M denaturant molar ellipticity intercepts for the native state and the denatured state baselines, respectively; and S_N and S_D are the slopes of the native state and the denatured state baselines, respectively. ΔG_0 and m describe the linear function of the unfolding free energy *versus* denaturant concentration. The effect of a given mutation on the stability of the protein ($\Delta\Delta G$) was calculated by taking the difference between the C_m value for WT* proteins and the C_m value for mutant proteins and multiplying by the average of the m values, as described by Pace and Scholtz and for which a negative value indicates a stabilizing mutation:[19]

$$\Delta\Delta G = (C_{m\ WT} - C_{m\ mutant})(m_{WT} + m_{mutant})/2 \quad (2)$$

Folding kinetics measurements

Initial studies using manual mixing indicated that the relaxation times for folding were more appropriate for stopped-flow data collection. Denatured protein samples were prepared by overnight dialysis against ADA buffer containing 2.5 M GuHCl. All folding kinetics data were collected using a KinTek SF2000 stopped-flow system (KinTek Corp., Austin, TX). Folding was initiated by a 1:10 dilution of 40 μM denatured protein into ADA buffer, with denaturant concentrations varying in increments of 0.05 M or 0.1 M, to the midpoint of denaturation as determined by the above described isothermal equilibrium denaturation measurements. The data collection strategy was designed to span approximately five half-lives, or >97% of the expected fluorescence signal change between the fully denatured state and the native state.

Unfolding kinetics measurements

Unfolding kinetics measurements were performed using a manual mixing technique. Protein samples (~30 μM) were dialyzed against ADA buffer overnight at 298 K. Unfolding was initiated by a 1:10 dilution into ADA buffer with a final GuHCl concentration of 1.5–5.5 M in 0.5-M increments. All unfolding data were collected using a Varian Eclipse fluorescence spectrophotometer equipped with a Peltier controlled-temperature unit at 298 K. Data collection times for each protein were designed so as to quantify the fluorescence signal over three to four half-lives, or >93% of the total expected amplitude.

Folding and unfolding kinetics analysis

The folding and unfolding characteristics of FGF-1 have previously been described in detail.[20] Briefly, the unfolding kinetics data exhibit an excellent fit to single exponential decay at all denaturant concentrations. The folding kinetics data also exhibit an excellent fit to a single exponential model, but only for denaturant concentrations above approximately 0.6 M GuHCl. Below this concentration, the folding kinetics data exhibit biexponential properties, with the slow phase being generally independent of denaturant concentration. The fast phase of this biexponential folding regime lies on the extrapolated region of the single-exponential folding data. Thus, the folding constant is derived from a fit to the monoexponential region and the fast phase of the biexponential region. Studies with WT FGF-1 have shown that the ΔG values derived from the folding and unfolding kinetics data are in excellent agreement with the values obtained from isothermal equilibrium denaturation data (monitored by fluorescence and circular dichroism), as well as differential

scanning calorimetry under varying concentrations of GuHCl denaturant.[20]

Both folding and unfolding kinetics data were collected in triplicate at each GuHCl concentration; data from at least three separate experiments were averaged in each case. The kinetics rates and amplitudes *versus* denaturant concentration were calculated from the time-dependent change in tryptophan fluorescence using a single exponential model:

$$I(t) = A\exp(-kt) + C \quad (3)$$

where $I(t)$ is the intensity of fluorescent signal at time t, A is the corresponding amplitude, k is the observed rate constant for the reaction, and C is a constant corresponding to the asymptotic signal limit. Folding and unfolding rate constant data were fitted to a global function describing the contribution of both rate constants to the observed kinetics as a function of denaturant ("chevron" plot) as described by Fersht:[32]

$$\ln(k_{obs}) = \ln(k_{f0}\exp(m_{k_f}D) + k_{u0}\exp(m_{k_u}D)) \quad (4)$$

where k_{f0} and k_{u0} are the folding and unfolding rate constants, respectively, extrapolated to 0 M denaturant; and m_{k_f} and m_{k_u} are the slopes of the linear functions relating $\ln(k_f)$ and $\ln(k_u)$, respectively, to denaturant concentration [D]. The Gibbs energy changes $\Delta\Delta G_f$ and $\Delta\Delta G_u$ associated with mutational effects on the folding and unfolding kinetics constants, respectively, were determined by:

$$\Delta\Delta G_f = -RT\ln(k_{f\ WT}/k_{f\ mutant}) \quad (5)$$

and

$$\Delta\Delta G_u = -RT\ln(k_{u\ WT}/k_{u\ mutant}) \quad (6)$$

where k_f and k_u kinetics constants are determined at the average midpoint of denaturation for the reference and mutant proteins, respectively. ϕ value analysis followed the procedure of Fersht *et al.*:[22]

$$\phi_f = \Delta\Delta G_f/\Delta\Delta G \quad (7)$$

$$\phi_u = \Delta\Delta G_u/-\Delta\Delta G \quad (8)$$

where $\Delta\Delta G$ is determined from the isothermal equilibrium data (Eq. (2)).

Crystallization of FGF-1 mutants, X-ray data collection, and refinement

Purified protein for crystallization trials was dialyzed against 50 mM sodium phosphate, 100 mM NaCl, 10 mM ammonium sulfate, and 2 mM DTT (pH 7.5) ("crystallization buffer"), and concentrated to 10–20 mg/ml depending on the solubility of the mutant protein. Crystals were grown at room temperature using the hanging-drop vapor-diffusion method with 8 μl drop size and 1 ml of reservoir solution. Diffraction quality crystals typically grew within 1–2 weeks. The Leu26Asn/Asp28Asn/His93Gly mutant was crystallized in 18% polyethylene glycol 4000, 0.1 M Na Hepes (pH 7.5), and 12% isopropanol. Crystals of Asp70Ala/His93Gly were obtained from 25% polyethylene glycol 4000 and 0.1 M Bicine (*N*,*N*-bis(2-hydroxyethyl)glycine; pH 9.5). All other mutant proteins were crystallized from 2.5 to 4.0 M sodium formate in the presence of 0.2–1.0 M ammonium sulfate.

Diffraction data were collected at either the Southeast Regional Collaborative Access Team (SER-CAT) 22-BM beam line (λ = 1.00 Å) at the Advanced Photon Source, Argonne National Laboratory, using a MarCCD225 detector (Mar USA, Evanston, IL), or at the X25 beam line of the National Synchrotron Light Source at Brookhaven National Laboratory, using an ADSC Q315 CCD detector. In all cases, crystals were mounted and maintained in a stream of gaseous nitrogen at 100 K. Data were integrated and scaled with HKL2000 software.[33,34] His-tagged WT FGF-1 (PDB code 1JQZ) and His93Gly mutant of FGF-1 (PDB code 1K5U) were used as the search models in molecular replacement using the CNS software suite.[35] Model building and visualization utilized the O molecular graphics program.[36] Structure refinement utilized the CNS software suite, with 5% of the data in the reflection files set aside for R_{free} calculations.[37]

Protein Bank accession numbers

Coordinates and structure factors have been deposited in the PDB with accession numbers 3BAO, 3BA5, 3BA7, 3BAQ, 3BAU, 3BAV, 3B9U, 3BB2, 3BA4, 3BAD, 3BAG, and 3BAH.

Acknowledgements

Use of the Advanced Photon Source was supported by the US Department of Energy, Office of Science, Office of Basic Energy Sciences, under contract no. W-31-109-Eng-38. Use of SER-CAT 22-BM beam line at the Advanced Photon Source, Argonne National Laboratory, is acknowledged, and supporting institutions of SER-CAT may be found at www.ser-cat.org/members.html. Use of the National Synchrotron Light Source, Brookhaven National Laboratory, is acknowledged, and financial support comes principally from the Office of Biological and Environmental Research and the Office of Basic Energy Sciences of the US Department of Energy, and the National Center for Research Resources of the National Institutes of Health. All X-ray structures have been deposited in the PDB. This work was supported by a grant from the National Science Foundation (MCB 0314740).

Supplementary Data

Supplementary data associated with this article can be found, in the online version, at doi:10.1016/j.jmb.2008.01.055

References

1. Richardson, J. S. (1981). The anatomy and taxonomy of protein structure. *Adv. Protein Chem.* **34**, 167–339.
2. Sibanda, B. L., Blundell, T. L. & Thornton, J. M. (1989). Conformation of β-hairpins in protein structures. A systematic classification with applications to modelling by homology, electron density fitting and protein engineering. *J. Mol. Biol.* **206**, 759–777.

3. Gunasekaran, K., Ramakrishnan, C. & Balaram, P. (1997). Beta-hairpins in proteins revisited: lessons for de novo design. *Protein Eng.* **10**, 1131–1141.
4. Hutchinson, E. G. & Thornton, J. M. (1994). A revised set of potentials for beta-turn formation in proteins. *Protein Sci.* **3**, 2207–2216.
5. Guruprasad, K. & Rajkumar, S. (2000). β- and γ-turns in proteins revisited: a new set of amino acid turn-type dependent positional preferences and potentials. *J. Biosci.* **25**, 143–156.
6. Blandl, T., Cochran, A. G. & Skelton, N. J. (2003). Turn stability in β-hairpin peptides: investigation of peptides containing 3:5 type I G1 bulge turns. *Protein Sci.* **12**, 237–247.
7. Wan, W.-Y. & Milner-White, E. J. (1999). A natural grouping of motifs with an aspartate or asparagine residue forming two hydrogen bonds to residues ahead in sequence: their occurrence at a-helical N termini and in other situations. *J. Mol. Biol.* **286**, 1633–1649.
8. de Alba, E., Jimenez, M. A. & Rico, M. (1997). Turn residue sequence determines beta-hairpin conformation in designed peptides. *J. Am. Chem. Soc.* **119**, 175–183.
9. Santiveri, C. M., Jimenez, M. A., Rico, M., Van Gunsteren, W. F. & Daura, X. (2004). Beta-hairpin folding and stability: molecular dynamics simulations of designed peptides in aqueous solution. *J. Pept. Sci.* **10**, 546–565.
10. Santiveri, C. M., Santoro, J., Rico, M. & Jimenez, M. A. (2004). Factors involved in the stability of isolated beta-sheets: turn sequence, beta-sheet twisting, and hydrophobic surface burial. *Protein Sci.* **13**, 1134–1147.
11. de Alba, E., Jimenez, M. A., Rico, M. & Nieto, J. L. (1996). Conformational investigations of designed short linear peptides able to fold into beta-hairpin structures in aqueous solution. *Fold. Des.* **1**, 133–144.
12. Zerella, R., Chen, P. Y., Evans, P. A., Raine, A. & Williams, D. H. (2000). Structural characterization of a mutant peptide derived from ubiquitin: implications for protein folding. *Protein Sci.* **9**, 2142–2150.
13. Jager, M., Zhang, Y., Bieschke, J., Nguyen, H., Dendle, M., Bowman, M. E. *et al.* (2006). Structure–function–folding relationship in a WW domain. *Proc. Natl Acad. Sci. USA*, **103**, 10648–10653.
14. Murzin, A. G., Lesk, A. M. & Chothia, C. (1992). β-Trefoil fold. Patterns of structure and sequence in the Kunitz inhibitors interleukins-1β and 1α and fibroblast growth factors. *J. Mol. Biol.* **223**, 531–543.
15. Blaber, M., DiSalvo, J. & Thomas, K. A. (1996). X-ray crystal structure of human acidic fibroblast growth factor. *Biochemistry*, **35**, 2086–2094.
16. Schlessinger, J., Plotnikov, A. N., Ibrahimi, O. A., Eliseenkova, A. V., Yeh, B. K., Yayon, A. *et al.* (2000). Crystal structure of a ternary FGF–FGFR–heparin complex reveals a dual role for heparin in FGFR binding and dimerization. *Mol. Cell. Biol.* **6**, 743–750.
17. Pellegrini, L., Burke, D. F., von Delft, F., Mulloy, B. & Blundell, T. L. (2000). Crystal structure of fibroblast growth factor receptor ectodomain bound to ligand and heparin. *Nature*, **407**, 1029–1034.
18. Dubey, V. K., Lee, J., Somasundaram, T., Blaber, S. & Blaber, M. (2007). Spackling the crack: stabilizing human fibroblast growth factor-1 by targeting the N- and C-terminus β-strand interactions. *J. Mol. Biol.* **371**, 256–268.
19. Pace, C. N. & Scholtz, J. M. (1997). Measuring the conformational stability of a protein. In Protein Structure: A Practical Approach (Creighton, T. E., ed), pp. 299–321, Oxford University Press, Oxford.
20. Kim, J., Brych, S. R., Lee, J., Logan, T. M. & Blaber, M. (2003). Identification of a key structural element for protein folding within β-hairpin turns. *J. Mol. Biol.* **328**, 951–961.
21. Brych, S. R., Blaber, S. I., Logan, T. M. & Blaber, M. (2001). Structure and stability effects of mutations designed to increase the primary sequence symmetry within the core region of a β-trefoil. *Protein Sci.* **10**, 2587–2599.
22. Fersht, A. R., Matouschek, A. & Serrano, L. (1992). The folding of an enzyme: I. Theory of protein engineering analysis of stability and pathway of protein folding. *J. Mol. Biol.* **224**, 771–782.
23. Sato, S., Religa, T. L. & Fersht, A. R. (2006). ϕ-Analysis of the folding of the B domain of protein A using multiple optical probes. *J. Mol. Biol.* **360**, 850–864.
24. Blaber, S. I., Culajay, J. F., Khurana, A. & Blaber, M. (1999). Reversible thermal denaturation of human FGF-1 induced by low concentrations of guanidine hydrochloride. *Biophys. J.* **77**, 470–477.
25. Culajay, J. F., Blaber, S. I., Khurana, A. & Blaber, M. (2000). Thermodynamic characterization of mutants of human fibroblast growth factor 1 with an increased physiological half-life. *Biochemistry*, **39**, 7153–7158.
26. Gimenez-Gallego, G., Conn, G., Hatcher, V. B. & Thomas, K. A. (1986). The complete amino acid sequence of human brain-derived acidic fibroblast growth factor. *Biochem. Biophys. Res. Commun.* **128**, 611–617.
27. Linemeyer, D. L., Menke, J. G., Kelly, L. J., Disalvo, J., Soderman, D., Schaeffer, M.-T. *et al.* (1990). Disulfide bonds are neither required, present, nor compatible with full activity of human recombinant acidic fibroblast growth factor. *Growth Factors*, **3**, 287–298.
28. Ortega, S., Schaeffer, M.-T., Soderman, D., DiSalvo, J., Linemeyer, D. L., Gimenez-Gallego, G. & Thomas, K. A. (1991). Conversion of cysteine to serine residues alters the activity, stability, and heparin dependence of acidic fibroblast growth factor. *J. Biol. Chem.* **266**, 5842–5846.
29. Copeland, R. A., Ji, H., Halfpenny, A. J., Williams, R.W., Thompson, K. C., Herber, W. K. *et al.* (1991). The structure of human acidic fibroblast growth factor and its interaction with heparin. *Arch. Biochem. Biophys.* **289**, 53–61.
30. Brych, S. R., Kim, J., Logan, T. M. & Blaber, M. (2003). Accommodation of a highly symmetric core within a symmetric protein superfold. *Protein Sci.* **12**, 2704–2718.
31. Eftink, M. R. (1994). The use of fluorescence methods to monitor unfolding transitions in proteins. *Biophys. J.* **66**, 482–501.
32. Fersht, A. R. (1999). *Kinetics of protein folding*. Structure and Mechanism in Protein Science, W.H. Freeman and Co., New York.
33. Otwinowski, Z. (1993). *Proceedings of the CCP4 Study Weekend: "Data Collection and Processing"*. SERC Daresbury Laboratory, England.
34. Otwinowski, Z. & Minor, W. (1997). Processing of X-ray diffraction data collected in oscillation mode. *Methods Enzymol.* **276**, 307–326.
35. Brunger, A. T., Adams, P. D., Clore, G. M., DeLano, W.L., Gros, P., Grosse-Kunstleve, R. W. *et al.* (1998). Crystallography and NMR system (CNS): a new software system for macromolecular structure determination. *Acta Crystallogr. Sect. D*, **54**, 905–921.
36. Jones, T. A., Zou, J. Y., Cowan, S. W. & Kjeldgaard, M. (1991). Improved methods for the building of protein models in electron density maps and the location of errors in these models. *Acta Crystallogr. Sect. A*, **47**, 110–119.
37. Brunger, A. T. (1992). Free *R* value: a novel statistical quantity for assessing the accuracy of crystal structures. *Nature*, **355**, 472–475.